

Beyond the Dirac Delta: Mitigating Diversity Collapse in Reinforcement Fine-Tuning for Versatile Image Generation

Jinmei Liu¹ Haoru Li¹ Zhenhong Sun² Chaofeng Chen³ Yatao Bian⁴
 Bo Wang¹ Daoyi Dong⁵ Chunlin Chen¹ Zhi Wang¹

Abstract

Reinforcement learning (RL) has emerged as a powerful paradigm for fine-tuning large-scale generative models, such as diffusion and flow models, to align with complex human preferences and user-specified tasks. A fundamental limitation remains *the curse of diversity collapse*, where the objective formulation and optimization landscape inherently collapse the policy to a Dirac delta distribution. To address this challenge, we propose **DRIFT** (**D**iveRsity-Incentivized Reinforcement **F**ine-Tuning for **V**ersatile **I**mage **G**eneration), an innovative framework that systematically incentivizes output diversity throughout the on-policy fine-tuning process, reconciling strong task alignment with high generation diversity to enhance versatility essential for applications that demand diverse candidate generations. We approach the problem across three representative perspectives: i) **sampling** a reward-concentrated subset that filters out reward outliers to prevent premature collapse; ii) **prompting** with stochastic variations to expand the conditioning space, and iii) **optimization** of the intra-group diversity with a potential-based reward shaping mechanism. Experimental results show that DRIFT achieves superior Pareto dominance regarding task alignment and generation diversity, yielding a 9.08% \sim 43.46% increase in diversity at equivalent alignment levels and a 59.65% \sim 65.86% increase in alignment at equivalent levels of diversity.

1. Introduction

With advancements in large-scale models trained on massive datasets, image generation models (e.g., diffusion and flow

¹Nanjing University ²Australia National University ³Wuhan University ⁴National University of Singapore ⁵University of Technology Sydney (jmliu@smail.nju.edu.cn, zhiwang@nju.edu.cn).

models) have demonstrated remarkable success in photorealistic image synthesis under diverse forms of guidance (Lipman et al., 2023; Dombrowski et al., 2025), including image-based (Zhang et al., 2024a), classifier-based (Dhariwal & Nichol, 2021), and text-based guidance (Rombach et al., 2022). Despite these advances, they are often deployed in scenarios that are not directly aligned with their likelihood-based training objectives. As a result, even state-of-the-art models (Podell et al., 2024; Betker et al., 2023) frequently exhibit misalignment with user prompts (Jiang et al., 2024) or human preferences (Xu et al., 2023). Recent studies explore using reinforcement learning (RL) to fine-tune image generation models by framing the multi-step denoising process as a sequential decision-making task (Fan et al., 2023; Black et al., 2024), achieving effective optimization for downstream tasks using only a black-box reward function (Wallace et al., 2024; Xue et al., 2025; Liu et al., 2025b).

However, a fundamental limitation of RL fine-tuning methods is *diversity collapse*, wherein the fine-tuned model achieves high rewards but loses output diversity, producing monotonous, single-pattern images (Barceló et al., 2024; Jena et al., 2025). This phenomenon is not merely a consequence of imperfect reward design but an inherent “curse” of the RL fine-tuning paradigm, as it continuously amplifies the likelihood of high-reward regions while substantially narrowing the model’s overall coverage (Yue et al., 2025). A natural remedy is to incorporate Kullback–Leibler (KL) regularization between the fine-tuned and pre-trained models, thereby discouraging over-optimization (Fan et al., 2023; Liu et al., 2025b). However, simply constraining the policy to the base model limits versatility in learning new content, resulting in suboptimal alignment to diverse downstream tasks (Hong et al., 2026). Recent studies (Jena et al., 2025; Sorokin et al., 2025; Gandikota & Bau, 2025; Sadat et al., 2024) adopt a range of sampling strategies to balance alignment and diversity, relying on hand-tuned heuristics for guided sampling at inference time and failing to address the fundamental problem of diversity collapse during RL fine-tuning. These limitations highlight the need for effective and computationally efficient schemes to address the diversity collapse challenge toward scaling RL compute for versatile image generation.

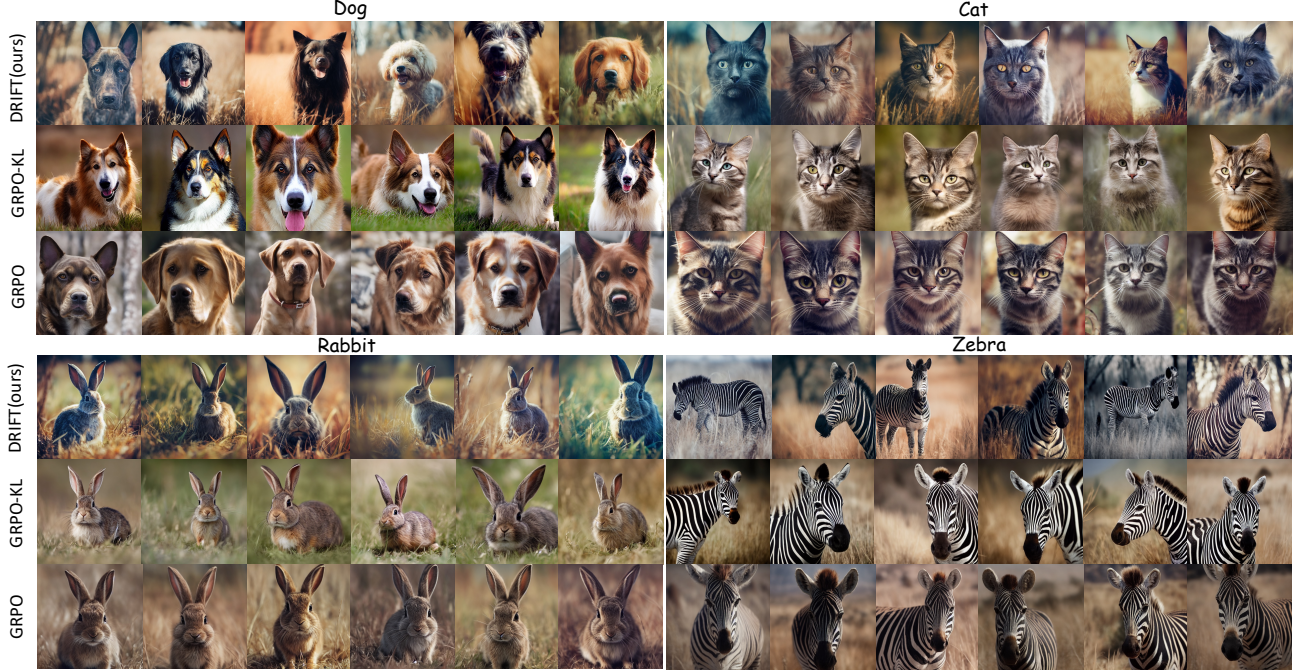


Figure 1. Image generation models fine-tuned via RL often suffer from *diversity collapse*, resulting in repetitive outputs with near-identical attributes in breeds, poses, and backgrounds. Instead, DRIFT maintains both high fidelity and diversity. The three sets were sampled using identical seeds and prompts, from fine-tuning SDv1.5 using PickScore as the reward function.

In this paper, we propose **DRIFT** (**D**iveRsi**t**-Incentivized **R**einforcement **F**ine-Tuning for **V**ersatile **I**mage **G**eneration), an innovative framework that systematically injects diversity incentives into RL fine-tuning to achieve both strong task alignment and high generation diversity, promoting versatility essential for applications that demand diverse candidate generations. We begin by analyzing *the curse of diversity collapse* within the mainstream paradigm, demonstrating how the objective formulation and optimization landscape inevitably collapse the policy to a Dirac delta distribution. This motivates us to explicitly embed diversity incentives into RL fine-tuning, facilitating the model to explore a broader manifold of diverse generations throughout the on-policy learning process. To this end, we approach the problem from three key dimensions: i) **sampling**, we sample a reward-concentrated subset for policy update, filtering out reward outliers to prevent premature collapse. ii) **prompting**, we introduce stochastic variations to prompt inputs, expanding the conditioning space from which image groups are generated; and iii) **optimization**, we formulate the intra-group diversity as an intrinsic reward and design a potential-based reward shaping scheme to preserve optimal policy invariance. We anticipate that this study will provide a coherent view for further research into diversity-preserving techniques for versatile image generation.

Experimental results show that DRIFT consistently achieves superior Pareto dominance regarding task alignment and

generation diversity across various reward models. Compared to competitive baselines, DRIFT yields a 9.08% \sim 43.46% increase in diversity at equivalent levels of alignment and a 59.65% \sim 65.86% increase in alignment at equivalent levels of diversity. Comprehensive analysis and case studies reveal that DRIFT effectively mitigates diversity collapse from various dimensions.

2. Related Work

RL Fine-Tuning of Generative Models. Methods can be roughly categorized into three kinds according to the reward function. The first kind uses differentiable reward functions and backpropagates the reward function gradient through the full sampling procedure (Prabhudesai et al., 2023; Clark et al., 2024; Jia et al., 2025). The second uses preference-based reward functions derived from human comparison data to align with human preferences, such as DPOK (Fan et al., 2023), Diffusion-DPO (Wallace et al., 2024), and Diffusion-KTO (Li et al., 2024). The third uses a general form of black-box reward functions. DDPO (Black et al., 2024) formulates a policy gradient algorithm to optimize diffusion models, followed by B²-DiffuRL (Hu et al., 2025) that tackles the sparse-reward challenge. Flow-GRPO (Liu et al., 2025b) first integrates online RL into flow matching models, with an ODE-to-SDE conversion to enable statistical sampling for exploration. DanceGRPO (Xue et al.,

2025) further scales RL to large and diverse prompt sets for visual generation tasks. The expanding studies underscore the efficacy and practical utility of RL fine-tuning for large-scale generative models (Uehara et al., 2024; Chen et al., 2024; Ye et al., 2024; Li et al., 2025; Zheng et al., 2025).

Diversity in Image Generation. Maintaining generation diversity has long been a central challenge in the field of image synthesis (Zhang et al., 2024b; Dombrowski et al., 2025). The standard remedy to preserve diversity is using KL regularization to constrain the deviation from the base model (Zhai et al., 2025; Ye et al., 2025), which can degrade the model’s versatility in learning new content (Hong et al., 2026). Barceló et al. (2024) proposes a hierarchical approach to preserve high-level diversity by only fine-tuning the low-level features at later denoising timesteps. Miao et al. (2024) fine-tunes diffusion models using only a diversity reward to enhance generation diversity, while requiring a set of unbiased images for reference. Another line approaches the problem by adopting various sampling strategies at inference time, such as condition-annealed sampling (Sadat et al., 2024), annealed importance guidance (Jena et al., 2025), and combined generation (Sorokin et al., 2025). However, these methods rely on hand-tuned heuristics for guided sampling and fail to address the fundamental problem of diversity collapse during RL fine-tuning.

DiverseGRPO (Liu et al., 2025a) and GARDO (He et al., 2025) are concurrent works closely related to our method. DiverseGRPO uses spectral clustering to identify novel visual modes and enforces stronger early-stage KL constraints to preserve diversity. GARDO mitigates reward hacking by penalizing uncertain samples more with a gated KL scheme, and reweights the advantages of high-quality samples with a diversity-based multiplier. In contrast, we delve into the curse of diversity collapse within the KL-constrained paradigm, tackling the challenge through a systematic framework spanning sampling, prompting, and optimization.

3. Preliminaries

3.1. Denoising as Sequential Decision-Making

Diffusion/flow models transform a data distribution $p(\mathbf{x}_0|\mathbf{c})$ over a dataset of samples \mathbf{x}_0 and prompts \mathbf{c} through a sequential Markovian forward process $q(\mathbf{x}_t|\mathbf{x}_{t-1})$ that iteratively adds noise to data. Sampling from a trained model θ begins with drawing a random $\mathbf{x}_T \sim \mathcal{N}(\mathbf{0}, \mathbf{I})$ and following the reverse process $p_\theta(\mathbf{x}_{t-1}|\mathbf{x}_t, \mathbf{c})$ to produce a trajectory $\{\mathbf{x}_T, \mathbf{x}_{T-1}, \dots, \mathbf{x}_0\}$ ending with the clean \mathbf{x}_0 .

practice (Rafailov et al., 2023; Liu et al., 2025b), RL fine-tuning of a pre-trained model is formulated as a KL-

constrained reward maximization problem as

$$J(\theta) = \mathbb{E}_{\mathbf{c}, \mathbf{x}_0 \sim p_\theta(\mathbf{x}_0|\mathbf{c})} [r(\mathbf{x}_0, \mathbf{c})] - \beta \cdot \mathbb{D}_{\text{KL}} [\pi_\theta(\mathbf{x}_0|\mathbf{c}) || \pi_{\text{ref}}(\mathbf{x}_0|\mathbf{c})], \quad (1)$$

where $r(\mathbf{x}_0, \mathbf{c})$ is the reward defined over the samples and prompts, and β controls the deviation from a reference policy π_{ref} , usually the initial pre-trained model. The iterative denoising process is mapped to an MDP as

$$\begin{aligned} \mathbf{s}_t &\triangleq (\mathbf{x}_t, \mathbf{c}, t), \quad \mathbf{a}_t \triangleq \mathbf{x}_{t-1}, \\ \pi(\mathbf{a}_t|\mathbf{s}_t) &\triangleq p_\theta(\mathbf{x}_{t-1}|\mathbf{x}_t, \mathbf{c}), \\ P(\mathbf{s}_{t+1}|\mathbf{s}_t, \mathbf{a}_t) &\triangleq (\delta_{\mathbf{c}}, \delta_{t-1}, \delta_{\mathbf{x}_{t-1}}), \\ R(\mathbf{s}_t, \mathbf{a}_t) &\triangleq \mathbb{1}(t=0) \cdot r(\mathbf{x}_0, \mathbf{c}), \end{aligned} \quad (2)$$

where $\mathbf{s}_t/\mathbf{a}_t$ denotes state/action, π is the policy, and δ_y is the Dirac delta distribution with nonzero density only at y . The generative model serves as the policy network π_θ and parameterizes the Markov transition kernel P .

3.2. Group Relative Policy Optimization (GRPO)

We build upon GRPO (Shao et al., 2024; Xue et al., 2025; Liu et al., 2025b) to estimate policy gradients for the objective in Eq. 1. Given a prompt \mathbf{c} , a group of G images $\{\mathbf{x}_0^1, \dots, \mathbf{x}_0^G\}$ is generated from the sampling distribution $p_{\theta_{\text{old}}}(\mathbf{x}_0|\mathbf{c})$ with previous parameters θ_{old} , yielding rewards $\{r_1, \dots, r_G\}$. The advantage for each sample \mathbf{x}_0^i is calculated from group-level comparisons as

$$A_i = \frac{r_i - \text{mean}(\{r_1, r_2, \dots, r_G\})}{\text{std}(\{r_1, r_2, \dots, r_G\})}. \quad (3)$$

The policy π_θ is then updated by maximizing:

$$\mathbb{E}_{\mathbf{c}, \mathbf{x}_0^i \sim p_{\theta_{\text{old}}}} \left[\frac{1}{G} \sum_{i=1}^G \sum_{t=0}^T \text{CLIP}(\rho_{t,i} A_i) - \beta \mathbb{D}_{\text{KL}} [\pi_\theta || \pi_{\text{ref}}] \right],$$

where $\rho_{t,i} = \frac{\pi_\theta(\mathbf{a}_{t,i}|\mathbf{s}_{t,i})}{\pi_{\theta_{\text{old}}}(\mathbf{a}_{t,i}|\mathbf{s}_{t,i})}$ is the importance sampling ratio at timestep t in sample \mathbf{x}_0^i . The clipped objective $\text{CLIP}(\rho_{t,i} A_i) = \min(\rho_{t,i} A_i, \text{clip}(\rho_{t,i}, 1 - \epsilon, 1 + \epsilon) A_i)$ ensures stable updates within the trust region (Schulman et al., 2017), where ϵ is a preset threshold constraining the discrepancy between the target policy π_θ and previous $\pi_{\theta_{\text{old}}}$.

4. The Curse of Diversity Collapse

Using a general derivation from reward-weighted regression (Peters & Schaal, 2007), the optimal solution to the reward maximization objective in Eq. 1 takes the form:

$$\pi^*(\mathbf{x}_0|\mathbf{c}) = \frac{1}{Z(\mathbf{c})} \pi_{\text{ref}}(\mathbf{x}_0|\mathbf{c}) \exp \left(\frac{1}{\beta} r(\mathbf{x}_0, \mathbf{c}) \right), \quad (4)$$

where $Z(\mathbf{c}) = \sum_{\mathbf{x}_0} \pi_{\text{ref}}(\mathbf{x}_0|\mathbf{c}) \exp(\frac{1}{\beta} r(\mathbf{x}_0, \mathbf{c}))$ is the partition function. Appendix B.1 presents a complete derivation.

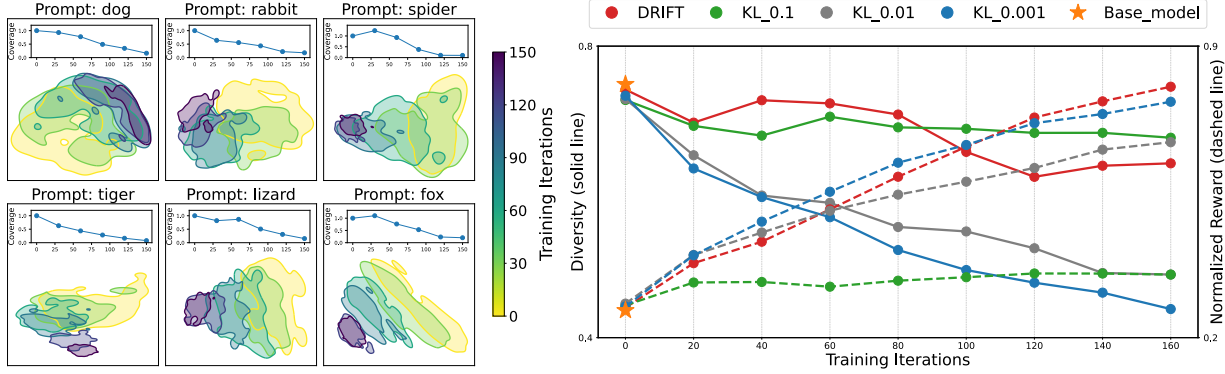


Figure 2. **Left:** Diversity collapse of the policy distribution $\pi_\theta(x_0|c)$ during GRPO fine-tuning, visualized by kernel density estimation contours of DreamSim embeddings, where the effective support area shrinks monotonically over training. **Right:** Comparison of reward-diversity tradeoffs, where DRIFT outperforms GRPO-KL by preserving significantly higher diversity at equivalent reward levels.

A large β leads to under-optimization, where the model becomes too conservative to effectively explore the reward landscape, ultimately failing to achieve significant gains in task alignment. Lowering β induces a rapid sharpening of the π^* distribution, as the exponential weighting term amplifies minor reward variations into massive probability gaps. When β approaches zero, i.e., the objective in Eq. 1 reduces to unconstrained reward maximization. Consequently, the model suffers from *total diversity collapse* as the policy converges to the singular maximum-reward mode as

$$\lim_{\beta \rightarrow 0^+} \pi_\beta^*(x_0|c) = \delta(x_0 - \arg \max_{x_0} r(x_0, c)), \quad (5)$$

where $\delta(\cdot)$ is the Dirac delta distribution that collapses all probability mass onto the origin. See Appendix B.2 for a complete proof.

From the optimization perspective, the policy gradient for the objective in Eq. 1 is derived as

$$\begin{aligned} \nabla_\theta J(\theta) &= \mathbb{E}_{\pi_\theta} \left[\nabla_\theta \log \pi_\theta \cdot \left(r - \beta \log \frac{\pi_\theta}{\pi_{\text{ref}}} \right) \right] \quad (6) \\ &= \mathbb{E}_{\pi_\theta} \left[\underbrace{\nabla_\theta \log \pi_\theta \cdot r}_{\text{Reward Pull}} - \underbrace{\beta \nabla_\theta \log \pi_\theta \cdot \log \frac{\pi_\theta}{\pi_{\text{ref}}}}_{\text{Diversity Push-back}} \right]. \end{aligned}$$

Since the *on-policy gradient* is calculated as an expectation over the current policy π_θ , as soon as π_θ shifts slightly toward a high-reward region, the model starts sampling from that region more frequently. The KL constraint only provides a push-back signal for samples generated from π_θ . Since the model stops seeing the low-reward but diverse regions, the gradient signal for those regions vanishes. Similar evidence can be found in (Ye et al., 2025). The on-policy nature often drives the model to exploit out-of-distribution regions from the data manifold, where π_{ref} lacks sufficient coverage and fails to provide reliable regularization. Multi-step Markovian sampling exacerbates this issue

as the discrepancy accumulates progressively throughout the sequential denoising trajectory.

The preceding analysis reveals that diversity collapse is: i) a fundamental mathematical limit inherent in the objective formulation (Eqs. 4-5), and ii) a manifestation of the local minima problem within the optimization landscape (Eq. 6). Figure 2 provides corresponding empirical evidence. Mitigating this curse is a prerequisite for scaling RL compute in versatile image generation.

5. Mitigating Diversity Collapse

In this section, we present DRIFT in detail, a coherent framework that enables versatile image generation by directly embedding diversity incentives into the on-policy fine-tuning process. We approach the goal from three key dimensions: sampling, prompting, and optimization, as described below.

5.1. Reward-Concentrated Sampling

As shown in Eq. 4, RL fine-tuning shifts the reference policy toward an optimal distribution through the exponential weighting term $\exp(\frac{1}{\beta} r(x_0, c))$. With a GRPO-based setting, substantial reward variances within a group are often amplified into significant probability gaps in the updated policy, thereby exacerbating diversity collapse. Inspired by this insight, we propose updating the policy using a reward-concentrated subset of samples, effectively filtering out reward outliers that would otherwise excessively sharpen the policy distribution.

Specifically, we adopt a simple selective sampling regime during fine-tuning. At each training iteration, the policy generates a pool of $2G$ candidate outputs for each prompt, from which G samples are selected to construct the training batch. For each candidate, we compute the cumulative reward distance to its $G - 1$ nearest neighbors. The sample yielding

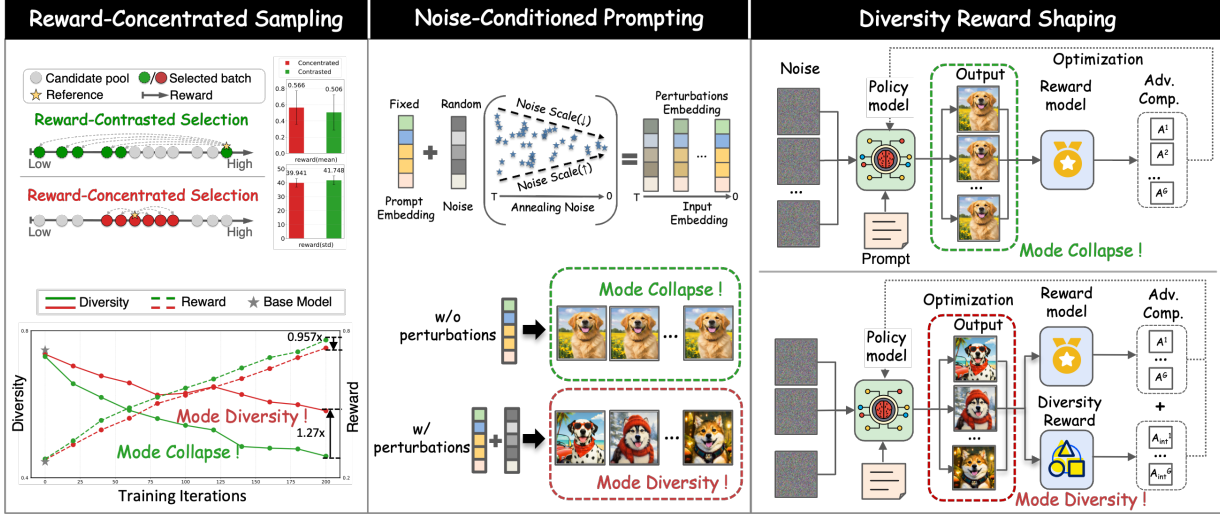


Figure 3. Overview of DRIFT: A unified framework for mitigating diversity collapse across the sampling, prompting, and optimization.

the minimal sum is identified as the reference point, and the training subset is constructed by grouping this reference with its $G - 1$ nearest neighbors. This procedure ensures a more concentrated reward distribution within the selected group. The details are provided in Appendix E.

5.2. Noise-Conditioned Prompting

Beyond sample selection, we investigate how inducing stochasticity at the prompting stage influences output diversity during RFT. Specifically, we introduce controlled noise perturbations to the prompt embeddings to induce a broader distribution of generated images. For a given prompt c , we add Gaussian noise to its embedding e at each denoising timestep t , resulting in a time-dependent perturbed prompt embedding \tilde{e}_t as

$$\tilde{e}_t = \sqrt{\gamma(t)} e + \eta \cdot \sqrt{1 - \gamma(t)} n, \quad n \sim \mathcal{N}(\mathbf{0}, \mathbf{I}), \quad (7)$$

where η controls the overall noise scale and $\gamma(t) \in [0, 1]$ is an annealing function that decreases with timestep t . In this manner, larger perturbations are applied at earlier timesteps and gradually reduced as the denoising process proceeds. The annealing schedule aligns prompt-level stochasticity with the diffusion dynamics, encouraging diverse global structures while preserving fine-grained semantic consistency at later stages. The details are provided in Appendix F.

5.3. Diversity Optimization via Reward Shaping

We incorporate the output diversity as an auxiliary objective, enabling its direct optimization throughout the training process. A straightforward approach is to include the intra-group diversity as an additional reward to guide fine-tuning. However, such naive reward shaping can shift the optimal policy, potentially misleading the model toward learning

suboptimal policies (Ng et al., 1999). Therefore, we employ a potential-based reward shaping scheme to allow for the inclusion of the intrinsic reward without distorting the original objective (Wang et al., 2023; Müller & Kudenko, 2025). Formally, we formulate the **intrinsic reward** R_{int} as the difference between the diversities of adjacent states as

$$R_{\text{int}}(s_t, a_t, s_{t+1}) = \gamma d(s_{t+1}) - d(s_t), \quad (8)$$

where the diversity function $d(\cdot)$ is exactly the potential function over states $s \in \mathcal{S}$. In the setting of the denoising MDP in Eq. 2, the specific intrinsic reward becomes

$$R_{\text{int}}((\mathbf{x}_t^i, \mathbf{c}, t), \mathbf{x}_{t-1}^i, (\mathbf{x}_{t-1}^i, \mathbf{c}, t-1)) = \gamma d(\mathbf{x}_{t-1}^i) - d(\mathbf{x}_t^i),$$

where $i = 1, \dots, G$. Since our method is built upon GRPO, it calculates policy gradients at the trajectory level, the intrinsic reward for a complete denoising process $\tau = (\mathbf{x}_T, \mathbf{x}_{T-1}, \dots, \mathbf{x}_0)$ is computed as

$$\begin{aligned} R_{\text{int}}(\tau^i) &= \sum_{t=0}^{T-1} \gamma^t R_{\text{int}}(s_t, a_t, s_{t+1}) \\ &= \sum_{t=0}^{T-1} \gamma^t [\gamma d(\mathbf{x}_{T-t-1}^i) - d(\mathbf{x}_{T-t}^i)], \\ &= \gamma^T d(\mathbf{x}_0^i) - d(\mathbf{x}_T^i), \\ &= \gamma^T d(\mathbf{x}_0^i), \end{aligned} \quad (9)$$

where we assume that the diversity of initial noise $\mathbf{x}_T \sim \mathcal{N}(\mathbf{0}, \mathbf{I})$ is zero, i.e., $d(\mathbf{x}_T^i) = 0$. The diversity of the final output $d(\mathbf{x}_0^i)$ is defined as the intra-group dissimilarity with respect to other samples within the same generation group.

Given a pair of output samples $(\mathbf{x}_0^i, \mathbf{x}_0^j)$ generated from the same prompt, we project them into a latent embedding space using an encoder \mathcal{E} and measure their dissimilarity using

the squared Euclidean distance between the corresponding embeddings:

$$d(\mathbf{x}_0^i, \mathbf{x}_0^j) = \left\| \mathcal{E}(\mathbf{x}_0^i) - \mathcal{E}(\mathbf{x}_0^j) \right\|^2. \quad (10)$$

We utilize DreamSim (Fu et al., 2023) as the encoder, as it is particularly well suited for RFT, which typically addresses downstream objectives such as text-image alignment and human-centric evaluation. For a group of samples $\{\mathbf{x}_0^1, \mathbf{x}_0^2, \dots, \mathbf{x}_0^G\}$, we compute their pairwise dissimilarities using the diversity metric in Eq. 10, resulting in a $G \times G$ matrix where the element in the i -th row and j -th column denotes the diversity between samples \mathbf{x}_0^i and \mathbf{x}_0^j . The diversity of sample \mathbf{x}_0^i within the group is obtained by averaging its dissimilarities to all other outputs, as

$$d(\mathbf{x}_0^i) = \frac{1}{G-1} \sum_{j=1, j \neq i}^G \left\| \mathcal{E}(\mathbf{x}_0^i) - \mathcal{E}(\mathbf{x}_0^j) \right\|^2. \quad (11)$$

A higher value of $d(\mathbf{x}_0^i)$ indicates that the i -th sample is less similar to the other outputs within the group, reflecting greater intra-group diversity. Appendix C provides additional details on intra-group diversity computation.

The diversity-incentivized intrinsic reward enables the model to maintain higher output diversity without compromising the primary objective of task alignment. This mechanism effectively prevents the fine-tuned model from collapsing into narrow solution modes, promoting a balanced tradeoff between generation quality and diversity. Accordingly, the new reward function is defined as

$$\tilde{R}(\tau^i) = R(\tau^i) + \lambda \cdot R_{\text{int}}(\tau^i), \quad (12)$$

where λ is the shaping ratio that balances between quality and diversity. Finally, we substitute the augmented reward function $\tilde{r}_i = \tilde{R}(\tau^i)$ for the original one $r_i = R(\tau^i)$ in Eq. 3 to compute the advantage under the GRPO framework.

Incorporating the intrinsic reward R_{int} will transform the original MDP $M = (\mathcal{S}, \mathcal{A}, P, R, \gamma)$ to a new one $\tilde{M} = (\mathcal{S}, \mathcal{A}, P, \tilde{R}, \gamma)$, where $\tilde{R} = R + \lambda R_{\text{int}}$. As we optimize a policy for the transformed MDP \tilde{M} with the intention of deploying it within the original MDP M , it is critical to ensure that the reward shaping does not bias the agent toward suboptimal solutions. Theorem 1 establishes that the optimal policy invariance is preserved when incorporating intra-group diversity as an intrinsic reward, providing a theoretical foundation for our reward shaping mechanism. Appendix A presents the detailed proof.

Theorem 1 (Optimal Policy Invariance). *Let $M = (\mathcal{S}, \mathcal{A}, P, R, \gamma)$ denote the MDP for the task of fine-tuning diffusion models with RL. $d(\cdot) : \mathcal{S} \mapsto \mathbb{R}$ is a real-valued*

function that computes the intra-group diversity $d(s)$ of the state s within a group of generation samples. We formulate $R_{\text{int}}(\cdot) : \mathcal{S} \times \mathcal{A} \times \mathcal{S} \mapsto \mathbb{R}$ as an intrinsic reward function that is the difference between the diversities of adjacent states, such that for all $s \in \mathcal{S}, a \in \mathcal{A}, s' \in \mathcal{S}$, $R_{\text{int}}(s, a, s') = \gamma d(s') - d(s)$. Then, with any constant balancing ratio λ , every optimal policy in the transformed MDP $\tilde{M} = (\mathcal{S}, \mathcal{A}, P, R + \lambda R_{\text{int}}, \gamma)$ will also be an optimal policy in M , and vice versa.

The ingenuity of our reward-shaping design lies in that, by setting the shaping reward as the difference between the diversities of adjacent states as in Eq. 8, the intrinsic reward for a complete denoising trajectory is derived as the diversity of the clean image as in Eq. 9. This elegant formulation bypasses the need to evaluate intermediate noised images, which significantly reduces computation while minimizing the influence of noisy factors on the diversity calculation.

Clipped Reward Shaping. Although DRIFT preserves optimal policy invariance after reward shaping, the model may still over-exploit intrinsic rewards at the expense of the primary objective, i.e., the *reward hacking* phenomenon, where an RL agent exploits flaws or ambiguities in the reward function to achieve high rewards without truly solving the intended task. Because the diversity reward is inherently high-variance and sensitive to outliers, noisy or low-quality outputs that deviate from the target manifold may produce disproportionately large diversity signals, potentially misguiding the optimization toward semantically dispersed but sub-optimal samples. To address this issue, we clip the diversity reward as

$$R_{\text{int}}(\tau^i) = \text{clip}(R_{\text{int}}(\tau^i), 0, \sigma), \quad (13)$$

where σ is a predetermined upper bound that prevents the model from excessively exploiting the shaping reward.

Decoupled Advantage Computation. During training, both the primary reward R and the intrinsic reward R_{int} evolve continuously as the policy improves, yet they typically operate on disparate and dynamically shifting scales. The magnitude of the intrinsic reward remains stable, since it is calculated based on the relative distance between samples within the group. However, the magnitude of the primary reward can vary substantially across different training stages and reward models. This complicates the development of a flexible weighting scheme for aggregating the two rewards as in Eq. 12. To circumvent this issue, we instead compute the advantages for each reward component independently, and merge them at the advantage level as

$$\tilde{A} = A + \lambda \cdot A_{\text{int}}. \quad (14)$$

By decoupling advantage estimation, each reward signal is normalized relative to its own baseline before aggregation.

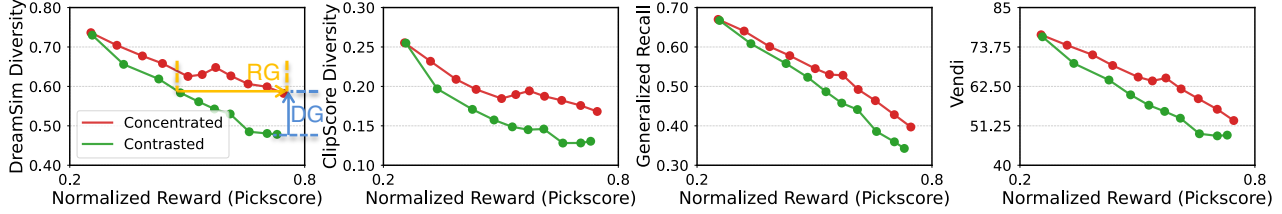


Figure 4. Comparison of reward-diversity tradeoff between reward-concentrated and reward-contrasted sampling, with SDv1.5 fine-tuned using PickScore reward. The record points in the Pareto frontier are collected from checkpoints at regular intervals during fine-tuning. **DG** denotes **Diversity Gain** at equivalent reward levels and **RG** denotes **Reward Gain** at equivalent diversity levels.² Both metrics are reported in the subsequent histograms (e.g., Figure 6) and tables (e.g., Table 1).

This architecture mitigates sensitivity to scale mismatch and temporal fluctuations, facilitating more robust and interpretable control over diversity regularization.

6. Experiments

Models. Following prior work (Black et al., 2024; Liu et al., 2025b), we consider Stable Diffusion v1.5 (SDv1.5) (Rombach et al., 2022) as the backbone model, which has been widely adopted in both academia and industry for text-to-image synthesis. The model is fine-tuned using LoRA (Hu et al., 2022) applied to the UNet’s attention layers (Ronneberger et al., 2015), reducing training overhead while maintaining performance. We employ the DDIM sampler with 50 sampling steps under an SDE-based stochastic formulation (Song et al., 2021), where noise is injected during the denoising process to enable randomized sampling and likelihood estimation. We use classifier-free guidance with a scale of 5, following common practice.

Evaluation Measures. Model evaluation is centered on both the alignment reward and generation diversity. We evaluate the fine-tuned models using images generated from a fixed set of representative prompts. We consider four metrics for a well-rounded assessment of generation diversity (See Appendix D for more details):

- **DreamSim Diversity**, it measures perceptual similarity between image pairs and is particularly well-suited for tasks focused on human-centric evaluation.
- **ClipScore Diversity**, it assesses the semantic diversity of the generated images using a CLIP model, focusing on the variety in high-level concepts.
- **Generalized Recall**, it evaluates how well the model covers the full distribution of possible outputs, indicating its ability to explore a wide range of diverse images.
- **Vendi Score**, it quantifies the effective number of distinct modes captured by the image distribution.

Baselines. We compare DRIFT to competitive RL fine-tuning baselines under identical experimental settings:

- **Base model** (Rombach et al., 2022): pretrained base models used in all experiments (SDv1.5).
- **DDPO** (Black et al., 2024): formulates a policy gradient algorithm to optimize diffusion models.
- **GRPO** (Shao et al., 2024): computes advantages from group-level comparisons to estimate policy gradients.
- **GRPO-KL** (Liu et al., 2025b): extends GRPO with KL regularization to prevent over-optimization.

All models are trained using two reward functions: **PickScore** (Kirstain et al., 2023) and **HPSv2** (Human Preference Score v2) (Wu et al., 2023), to align with human preferences and text relevance. Rewards are normalized to the unit interval [0, 1]. See Appendices G and H for details of the implementation of training and reward functions.

6.1. Study of Reward-Concentrated Sampling

We first verify the effectiveness of *reward-concentrated sampling* by comparing it against *reward-contrasted sampling*, an inverse strategy that updates the policy using a subset with maximal reward variance. This comparison offers intuitive insight into how sampling strategies govern the tradeoff between reward optimization and diversity preservation.

Figure 4 presents the Pareto frontiers of the opposite strategies during the fine-tuning process. Reward-concentrated sampling establishes a more favorable Pareto frontier. At equivalent reward levels, it preserves significantly higher image diversity across all four diversity metrics. Selecting a reward-concentrated subset filters out reward outliers that would otherwise excessively sharpen the policy distribution,

²When measuring RG, we maintain approximately equivalent diversity levels using DreamSim Diversity as the reference, as illustrated by the yellow line. Conversely, for DG, we maintain approximately equivalent reward levels, as indicated by the blue line. Since it is infeasible to obtain checkpoints that induce exactly the same reward or diversity values for different methods, we adopt a stringent comparison protocol by selecting checkpoints for DRIFT that slightly exceed the baseline’s coordinates. This approach confirms that our reported improvements represent a lower bound of the actual performance gap.

thereby facilitating more robust exploration of semantically meaningful behaviors for task alignment.

Figure 5 presents a qualitative analysis, demonstrating that our reward-concentrated sampling produces a broader distribution of image generations while preserving high visual fidelity compared to reward-contrast sampling. The quantitative results in Figure 6 substantiate this observation, demonstrating that the reward-concentrated setting achieves substantial improvements, specifically a diversity gain of $8.56\% \sim 30.77\%$ and a reward gain of 37.74%.



Figure 5. Qualitative diversity comparisons show that reward-concentrated sampling maintains high fidelity and achieves significantly greater diversity after fine-tuning SDv1.5 using PickScore.

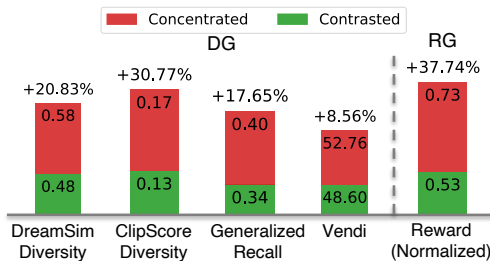


Figure 6. Diversity and Reward Gain of reward-concentrated over reward-contrast sampling, SDv1.5 fine-tuned with PickScore.

6.2. Study of Noise-Conditioned Prompting

To comprehensively evaluate the effect of noise-conditioned prompting, we investigate four ablations: 1) add noise to prompt embeddings at both the training and testing stages, 2) add noise at training only, 3) add noise at testing only, and

4) no noise. The noise schedule remains consistent across training and testing, as described in Sec. 5.2.

Figure 9 reports the resulting reward–diversity tradeoffs for the four ablations. We observe that injecting noise into prompt embeddings during training consistently yields higher generation diversity. This suggests that prompt-level stochasticity effectively broadens the conditioning space, thereby diversifying the output distribution for the fine-tuned policy. Interestingly, adding equivalent noise during testing does not noticeably enhance the model’s generation diversity. These results indicate that the key to maintaining diversity lies in training with prompting noise, which structures the model’s latent space and governs its exploration dynamics. Once trained with prompt-level noising, the model inherently retains its ability to generate diverse outputs, even when noise is omitted during testing.

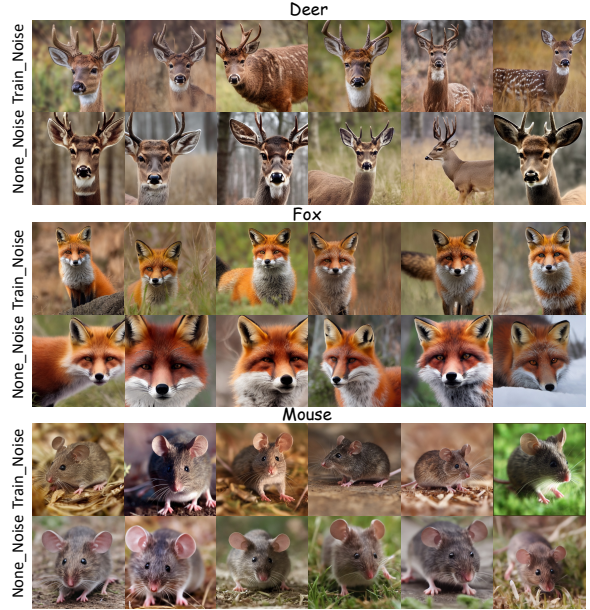


Figure 7. Qualitative diversity comparisons show that training with prompting noise maintains high fidelity while achieving significantly greater diversity after fine-tuning SDv1.5 using PickScore.

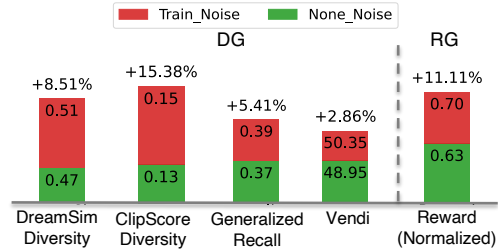


Figure 8. Diversity and Reward Gain of training w/ prompting noise over w/o noise, SDv1.5 fine-tuned with PickScore.

Figure 7 presents a qualitative analysis, where training with

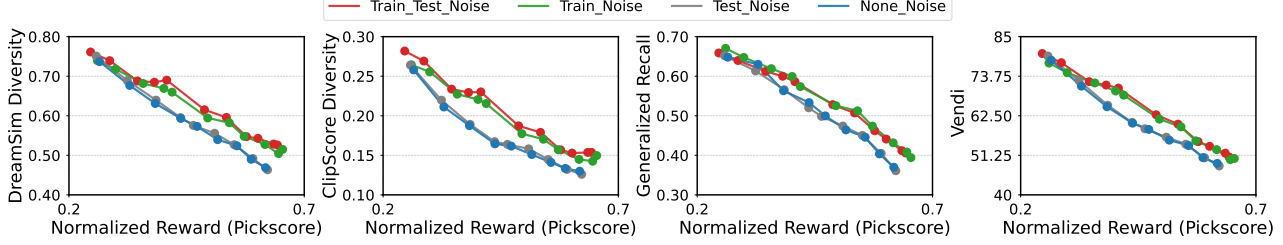


Figure 9. Comparison of reward-diversity tradeoff for prompting with and without noise, with SDv1.5 fine-tuned using PickScore reward.

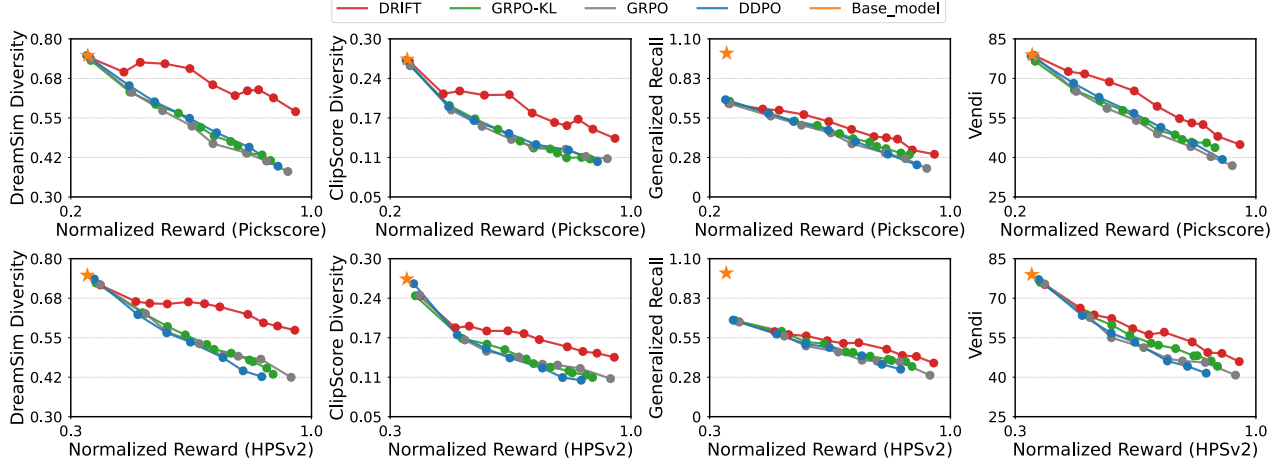


Figure 10. Reward-diversity comparison between DRIFT and baselines, with SDv1.5 fine-tuned using PickScore and HPSv2 rewards.

prompting noise demonstrates more diverse generations while maintaining high visual fidelity compared to omitting the noise. This finding is also supported by the quantitative results in Figure 8, which show a diversity gain of $2.86\% \sim 15.38\%$ and a reward gain of 11.11% achieved by our noise-conditioned prompting solution.

6.3. Study of Diversity-Aware Reward Shaping

Here, we evaluate DRIFT, which directly optimizes intra-group diversity via potential-based reward shaping, and demonstrate its superiority over competitive baselines. Figure 10 shows the Pareto frontiers of DRIFT against baselines for fine-tuning SDv1.5 using the PickScore and HPSv2 reward functions. GRPO-KL obtains a marginal advantage in diversity preservation over GRPO and DDPO. This improvement is attributed to KL regularization that encourages the policy to maintain the output distribution of the base model. In contrast, DRIFT establishes a significantly superior Pareto frontier compared to all baselines, demonstrating a more robust tradeoff between reward maximization and diversity preservation. The downward trend in diversity during RL fine-tuning is significantly attenuated, verifying that DRIFT effectively mitigates diversity collapse.

Table 1 summarizes the numerical results of DRIFT and the baselines. For both PickScore and HPSv2 setups, DRIFT achieves significant diversity gain in all four metrics compared to baselines. Particularly, DRIFT yields **a 40%+ diversity gain** in DreamSim Diversity and Generalized Recall trained with PickScore reward, and **a 30%+ diversity gain** in DreamSim and ClipScore Diversity trained with HPSv2 reward. The observed reward gain of $59.65\% \sim 65.86\%$ is particularly significant, highlighting DRIFT’s superior capability in aligning models with downstream task requirements. Qualitative visualizations in Figure 11 further demonstrate that DRIFT is capable of generating a diverse range of images while maintaining uncompromised image quality. Overall, DRIFT exhibits superior performance across both the reward and diversity dimensions, demonstrating its capacity to broaden the output diversity while not sacrificing the image quality at all.

6.4. Conclusion

In this paper, we delved into the curse of diversity collapse in RL fine-tuning of generative models, and proposed an innovative framework that systematically incentivizes output diversity for versatile image generation. Our method mitigates diversity collapse from three distinct dimensions: reward-

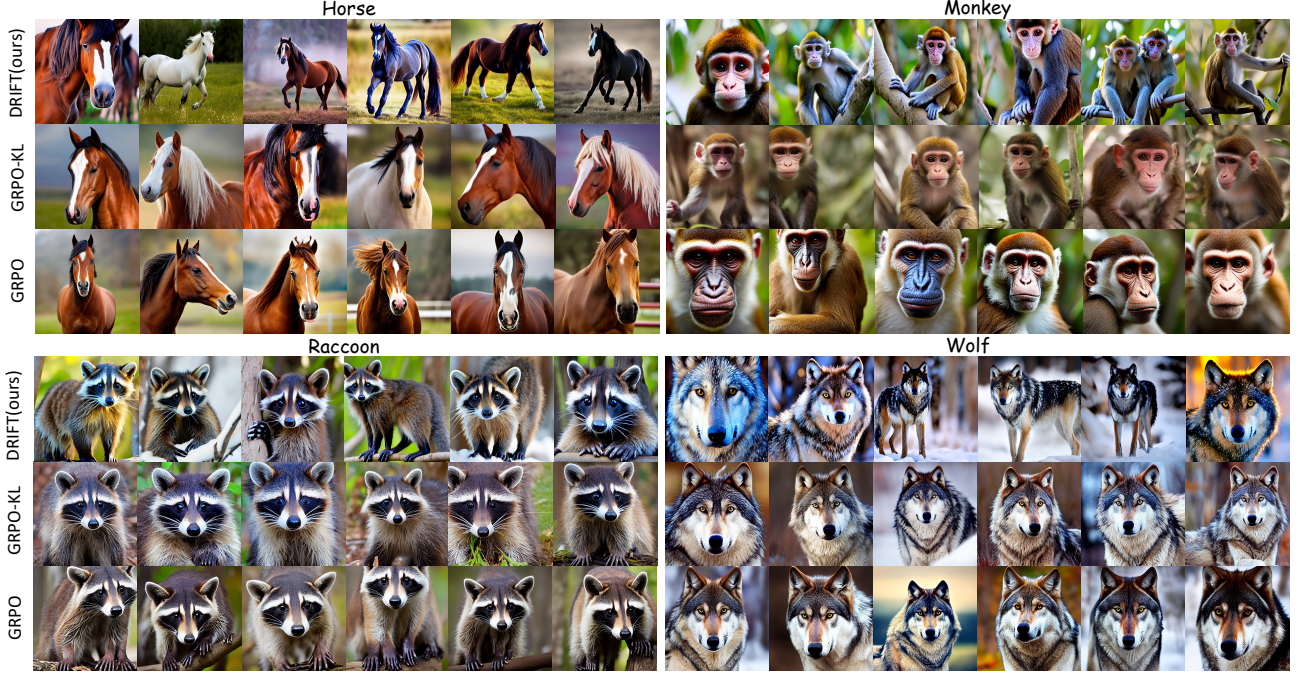


Figure 11. Qualitative diversity comparisons show that baseline methods suffer from diversity collapse, producing repetitive samples with similar breeds, poses, and backgrounds, whereas DRIFT maintains high fidelity with substantially greater diversity. All models are fine-tuned on SDv1.5 using HPSv2 as the reward function.

| Algorithm | Diversity (DG) | | | Quality (RG) | |
|----------------------------|-----------------------------------|------------------------------------|-----------------------------------|----------------------|------------------------------------|
| | DreamSim Diversity (\uparrow) | ClipScore Diversity (\uparrow) | Generalized Recall (\uparrow) | Vendi (\uparrow) | Reward (normalized) (\uparrow) |
| SD v1.5 / PickScore | | | | | |
| Base model | 0.7476 | 0.2678 | 1.0000 | 78.9582 | 0.2653 |
| DDPO | 0.3974 | 0.1058 | 0.2233 | 39.2261 | 0.5851 |
| GRPO | 0.3804 | 0.1105 | 0.1989 | 36.8989 | 0.5927 |
| GRPO-KL | 0.4153 | 0.1100 | 0.2945 | 43.7285 | 0.5503 |
| DRIFT | 0.5698 | 0.1426 | 0.3271 | 44.8873 | 0.9187 |
| DG / RG (avg.) | +43.46% | +31.16% | +40.68% | +12.91% | +59.65 % |
| SD v1.5 / HPSv2 | | | | | |
| Base model | 0.7476 | 0.2678 | 1.0000 | 78.9582 | 0.3016 |
| DDPO | 0.4267 | 0.1076 | 0.3303 | 41.5299 | 0.5400 |
| GRPO | 0.4245 | 0.1102 | 0.2883 | 40.7874 | 0.5409 |
| GRPO-KL | 0.4342 | 0.1120 | 0.3496 | 44.1385 | 0.5961 |
| DRIFT | 0.5737 | 0.1439 | 0.3734 | 45.9274 | 0.9252 |
| DG / RG (avg.) | +33.90% | +30.93% | +16.47% | +9.08% | +65.86 % |

Table 1. Comparison between baselines and our method on diversity and quality metrics under different reward functions.

concentrated sampling, noise-conditioned prompting, and diversity optimization via reward shaping. Comprehensive experimental results verify that our method consistently achieves superior Pareto frontiers, reconciling high generation diversity with strong task alignment. We hope that our analysis and framework will provide a coherent foundation for future research into diversity-preserving techniques for large-scale generative models.

A limitation of our approach is the reliance on an auxiliary module for calculating intra-group diversity, which may increase computational complexity. Future work could obviate the need for this external component by leveraging the model’s internal latent representations to derive diversity metrics. Another promising direction involves extending our approach to video and 3D generation, where the challenge of diversity collapse is equally prevalent.

References

Barceló, R., Alcázar, C., and Tobar, F. Avoiding mode collapse in diffusion models fine-tuned with reinforcement learning. *arXiv preprint arXiv:2410.08315*, 2024.

Betker, J., Goh, G., Jing, L., Brooks, T., Wang, J., Li, L., Ouyang, L., Zhuang, J., Lee, J., Guo, Y., et al. Improving image generation with better captions. *Computer Science*. <https://cdn.openai.com/papers/dall-e-3.pdf>, 2(3): 8, 2023.

Black, K., Janner, M., Du, Y., Kostrikov, I., and Levine, S. Training diffusion models with reinforcement learning. In *Proceedings of International Conference on Learning Representations*, 2024.

Chen, C., Wang, A., Wu, H., Liao, L., Sun, W., Yan, Q., and Lin, W. Enhancing diffusion models with text-encoder reinforcement learning. In *Proceedings of European Conference on Computer Vision*, pp. 182–198, 2024.

Clark, K., Vicol, P., Swersky, K., and Fleet, D. J. Directly fine-tuning diffusion models on differentiable rewards. In *Proceedings of International Conference on Learning Representations*, 2024.

Dhariwal, P. and Nichol, A. Diffusion models beat GANs on image synthesis. In *Advances in Neural Information Processing Systems*, volume 34, pp. 8780–8794, 2021.

Dombrowski, M., Zhang, W., Cechnicka, S., Reynaud, H., and Kainz, B. Image generation diversity issues and how to tame them. In *Proceedings of the Computer Vision and Pattern Recognition Conference*, pp. 3029–3039, 2025.

Fan, Y., Watkins, O., Du, Y., Liu, H., Ryu, M., Boutilier, C., Abbeel, P., Ghavamzadeh, M., Lee, K., and Lee, K. DPOK: Reinforcement learning for fine-tuning text-to-image diffusion models. In *Advances in Neural Information Processing Systems*, volume 36, pp. 79858–79885, 2023.

Friedman, D. and Dieng, A. B. The vendi score: A diversity evaluation metric for machine learning. *arXiv preprint arXiv:2210.02410*, 2022.

Fu, S., Tamir, N., Sundaram, S., Chai, L., Zhang, R., Dekel, T., and Isola, P. DreamSim: Learning new dimensions of human visual similarity using synthetic data. *arXiv preprint arXiv:2306.09344*, 2023.

Gandikota, R. and Bau, D. Distilling diversity and control in diffusion models. *arXiv preprint arXiv:2503.10637*, 2025.

He, H., Ye, Y., Liu, J., Liang, J., Wang, Z., Yuan, Z., Wang, X., Mao, H., Wan, P., and Pan, L. GARD: Reinforcing diffusion models without reward hacking. *arXiv preprint arXiv:2512.24138*, 2025.

Hong, J., Paul, S., Lee, N., Rasul, K., Thorne, J., and Jeong, J. Margin-aware preference optimization for aligning diffusion models without reference. In *AAAI Conference on Artificial Intelligence*, 2026.

Hu, E. J., Wallis, P., Allen-Zhu, Z., Li, Y., Wang, S., Wang, L., Chen, W., et al. Lora: Low-rank adaptation of large language models. In *Proceedings of International Conference on Learning Representations*, 2022.

Hu, Z., Zhang, F., Chen, L., Kuang, K., Li, J., Gao, K., Xiao, J., Wang, X., and Zhu, W. Towards better alignment: Training diffusion models with reinforcement learning against sparse rewards. In *Proceedings of the IEEE/CVF Conference on Computer Vision and Pattern Recognition*, pp. 23604–23614, 2025.

Ilharco, G., Wortsman, M., Carlini, N., Taori, R., Dave, A., Shankar, V., Namkoong, H., Miller, J., Hajishirzi, H., Farhadi, A., et al. Openclip. *Zenodo*, 2021.

Jena, R., Taghibakhshi, A., Jain, S., Shen, G., Tajbakhsh, N., and Vahdat, A. Elucidating optimal reward-diversity tradeoffs in text-to-image diffusion models. In *Proceedings of the IEEE/CVF Winter Conference on Applications of Computer Vision*, pp. 232–242. IEEE, 2025.

Jia, Z., Nan, Y., Zhao, H., and Liu, G. Reward fine-tuning two-step diffusion models via learning differentiable latent-space surrogate reward. In *Proceedings of the IEEE/CVF Conference on Computer Vision and Pattern Recognition*, pp. 12912–12922, 2025.

Jiang, D., Song, G., Wu, X., Zhang, R., Shen, D., Zong, Z., Liu, Y., and Li, H. Comat: Aligning text-to-image diffusion model with image-to-text concept matching. In *Advances in Neural Information Processing Systems*, volume 37, pp. 76177–76209, 2024.

Kirstain, Y., Polyak, A., Singer, U., Matiana, S., Penna, J., and Levy, O. Pick-a-pic: An open dataset of user preferences for text-to-image generation. In *Advances in Neural Information Processing Systems*, volume 36, pp. 36652–36663, 2023.

Kynkänniemi, T., Karras, T., Laine, S., Lehtinen, J., and Aila, T. Improved precision and recall metric for assessing generative models. In *Advances in Neural Information Processing Systems*, volume 32, 2019.

Li, S., Kallidromitis, K., Gokul, A., Kato, Y., and Kozuka, K. Aligning diffusion models by optimizing human utility. In *Advances in Neural Information Processing Systems*, volume 37, pp. 24897–24925, 2024.

Li, Y., Wang, Y., Zhu, Y., Zhao, Z., Lu, M., She, Q., and Zhang, S. BranchGRPO: Stable and efficient grpo with structured branching in diffusion models. *arXiv preprint arXiv:2509.06040*, 2025.

Lipman, Y., Chen, R. T., Ben-Hamu, H., Nickel, M., and Le, M. Flow matching for generative modeling. In *Proceedings of International Conference on Learning Representations*, 2023.

Liu, H., Huang, H., Wang, J., Liu, C., Li, X., and Ji, X. DiverseGRPO: Mitigating mode collapse in image generation via diversity-aware grpo. *arXiv preprint arXiv:2512.21514*, 2025a.

Liu, J., Liu, G., Liang, J., Li, Y., Liu, J., Wang, X., Wan, P., Zhang, D., and Ouyang, W. Flow-GRPO: Training flow matching models via online RL. *arXiv preprint arXiv:2505.05470*, 2025b.

Miao, Z., Wang, J., Wang, Z., Yang, Z., Wang, L., Qiu, Q., and Liu, Z. Training diffusion models towards diverse image generation with reinforcement learning. In *Proceedings of the IEEE/CVF Conference on Computer Vision and Pattern Recognition*, pp. 10844–10853, 2024.

Müller, H. and Kudenko, D. Improving the effectiveness of potential-based reward shaping in reinforcement learning. In *Proceedings of International Conference on Autonomous Agents and Multiagent Systems*, pp. 2684–2686, 2025.

Ng, A. Y., Harada, D., and Russell, S. J. Policy invariance under reward transformations: Theory and application to reward shaping. In *Proceedings of International Conference on Machine Learning*, pp. 278–287, 1999.

Peters, J. and Schaal, S. Reinforcement learning by reward-weighted regression for operational space control. In *Proceedings of International Conference on Machine Learning*, pp. 745–750, 2007.

Podell, D., English, Z., Lacey, K., Blattmann, A., Dockhorn, T., Müller, J., Penna, J., and Rombach, R. SDXL: Improving latent diffusion models for high-resolution image synthesis. In *Proceedings of International Conference on Learning Representations*, 2024.

Prabhudesai, M., Goyal, A., Pathak, D., and Fragkiadaki, K. Aligning text-to-image diffusion models with reward backpropagation. *arXiv preprint arXiv:2310.03739*, 2023.

Rafailov, R., Sharma, A., Mitchell, E., Manning, C. D., Ermon, S., and Finn, C. Direct preference optimization: Your language model is secretly a reward model. In *Advances in Neural Information Processing Systems*, volume 36, pp. 53728–53741, 2023.

Rombach, R., Blattmann, A., Lorenz, D., Esser, P., and Ommer, B. High-resolution image synthesis with latent diffusion models. In *Proceedings of the IEEE/CVF conference on computer vision and pattern recognition*, pp. 10684–10695, 2022.

Ronneberger, O., Fischer, P., and Brox, T. U-net: Convolutional networks for biomedical image segmentation. In *Proceedings of International Conference on Medical image computing and computer-assisted intervention*, pp. 234–241. Springer, 2015.

Sadat, S., Buhmann, J., Bradley, D., Hilliges, O., and Weber, R. M. CADS: Unleashing the diversity of diffusion models through condition-annealed sampling. In *Proceedings of International Conference on Learning Representations*, 2024.

Sajjadi, M. S., Bachem, O., Lucic, M., Bousquet, O., and Gelly, S. Assessing generative models via precision and recall. In *Advances in Neural Information Processing Systems*, volume 31, 2018.

Schulman, J., Wolski, F., Dhariwal, P., Radford, A., and Klimov, O. Proximal policy optimization algorithms. *arXiv preprint arXiv:1707.06347*, 2017.

Shao, Z., Wang, P., Zhu, Q., Xu, R., Song, J., Bi, X., Zhang, H., Zhang, M., Li, Y., et al. Deepseekmath: Pushing the limits of mathematical reasoning in open language models. *arXiv preprint arXiv:2402.03300*, 2024.

Song, J., Meng, C., and Ermon, S. Denoising diffusion implicit models. In *Proceedings of International Conference on Learning Representations*, 2021.

Sorokin, D., Nakhodnov, M., Kuznetsov, A., and Alanov, A. Imageref1: Balancing quality and diversity in human-aligned diffusion models. *arXiv preprint arXiv:2505.22569*, 2025.

Sutton, R. S. and Barto, A. G. *Reinforcement Learning: An Introduction*. The MIT Press, second edition, 2018.

Uehara, M., Zhao, Y., Biancalani, T., and Levine, S. Understanding reinforcement learning-based fine-tuning of diffusion models: A tutorial and review. *arXiv preprint arXiv:2407.13734*, 2024.

Wallace, B., Dang, M., Rafailov, R., Zhou, L., Lou, A., Purushwalkam, S., Ermon, S., Xiong, C., Joty, S., and Naik, N. Diffusion model alignment using direct preference optimization. In *Proceedings of the IEEE/CVF Conference on Computer Vision and Pattern Recognition*, pp. 8228–8238, 2024.

Wang, Y., Yang, M., Dong, R., Sun, B., Liu, F., et al. Efficient potential-based exploration in reinforcement learning using inverse dynamic bisimulation metric. In *Advances in Neural Information Processing Systems*, volume 36, pp. 38786–38797, 2023.

Wu, X., Hao, Y., Sun, K., Chen, Y., Zhu, F., Zhao, R., and Li, H. Human preference score v2: A solid benchmark for

evaluating human preferences of text-to-image synthesis. *arXiv preprint arXiv:2306.09341*, 2023.

Xu, J., Liu, X., Wu, Y., Tong, Y., Li, Q., Ding, M., Tang, J., and Dong, Y. Imagereward: Learning and evaluating human preferences for text-to-image generation. In *Advances in Neural Information Processing Systems*, volume 36, pp. 15903–15935, 2023.

Xue, Z., Wu, J., Gao, Y., Kong, F., Zhu, L., Chen, M., Liu, Z., Liu, W., Guo, Q., Huang, W., et al. Dancegrpo: Unleashing grp on visual generation. *arXiv preprint arXiv:2505.07818*, 2025.

Ye, H., Zheng, K., Xu, J., Li, P., Chen, H., Han, J., Liu, S., Zhang, Q., Mao, H., Hao, Z., et al. Data-regularized reinforcement learning for diffusion models at scale. *arXiv preprint arXiv:2512.04332*, 2025.

Ye, J., Liu, F., Li, Q., Wang, Z., Wang, Y., Wang, X., Duan, Y., and Zhu, J. DreamReward: Text-to-3d generation with human preference. In *Proceedings of European Conference on Computer Vision*, pp. 259–276. Springer, 2024.

Yue, Y., Chen, Z., Lu, R., Zhao, A., Wang, Z., Song, S., and Huang, G. Does reinforcement learning really incentivize reasoning capacity in LLMs beyond the base model? In *Advances in Neural Information Processing Systems*, 2025.

Zhai, K., Singh, U., Thatipelli, A., Chakraborty, S., Sahu, A. K., Huang, F., Bedi, A. S., and Shah, M. MIRA: Towards mitigating reward hacking in inference-time alignment of T2I diffusion models. *arXiv preprint arXiv:2510.01549*, 2025.

Zhang, W., Zang, C., Li, L., Cechnicka, S., Ouyang, C., and Kainz, B. Stability and generalizability in SDE diffusion models with measure-preserving dynamics. In *Advances in Neural Information Processing Systems*, volume 37, pp. 81606–81644, 2024a.

Zhang, Y., Tzeng, E., Du, Y., and Kislyuk, D. Large-scale reinforcement learning for diffusion models. In *Proceedings of European Conference on Computer Vision*, pp. 1–17, 2024b.

Zheng, K., Chen, H., Ye, H., Wang, H., Zhang, Q., Jiang, K., Su, H., Ermon, S., Zhu, J., and Liu, M.-Y. DiffusionNFT: Online diffusion reinforcement with forward process. *arXiv preprint arXiv:2509.16117*, 2025.

A. Optimal Policy Invariance in DRIFT

Following the classical reward shaping study (Ng et al., 1999), we give the proof of Theorem 1, which guarantees the optimal policy invariance when incorporating the intra-group diversity as an intrinsic reward.

Theorem 1 (Optimal Policy Invariance). *Let $M = (\mathcal{S}, \mathcal{A}, P, R, \gamma)$ denote the MDP for the task of fine-tuning diffusion models with RL. $d(\cdot) : S \mapsto \mathbb{R}$ is a real-valued function that computes the intra-group diversity $d(s)$ of the state s within a group of generation samples. We formulate $R_{\text{int}}(\cdot) : S \times \mathcal{A} \times S \mapsto \mathbb{R}$ as an intrinsic reward function that is the difference between the diversities of adjacent states, such that for all $s \in S, a \in \mathcal{A}, s' \in S$, $R_{\text{int}}(s, a, s') = \gamma d(s') - d(s)$. Then, with any constant balancing ratio λ , every optimal policy in the transformed MDP $\tilde{M} = (\mathcal{S}, \mathcal{A}, P, R + \lambda R_{\text{int}}, \gamma)$ will also be an optimal policy in M , and vice versa.*

Proof. For the original MDP M , we know that its optimal Q-function Q_M^* satisfies the Bellman optimality equation (Sutton & Barto, 2018):

$$Q_M^*(s, a) = \mathbb{E}_{s'} \left[R(s, a, s') + \gamma \max_{a' \in \mathcal{A}} Q_M^*(s', a') \right]. \quad (15)$$

With some simple algebraic manipulation, we can get:

$$Q_M^*(s, a) - \lambda d(s) = \mathbb{E}_{s'} \left[R(s, a, s') + \lambda (\gamma d(s') - d(s)) + \gamma \max_{a' \in \mathcal{A}} (Q_M^*(s', a') - \lambda d(s')) \right]. \quad (16)$$

If we now define $\hat{Q}_{\tilde{M}}(s, a) \triangleq Q_M^*(s, a) - \lambda d(s)$ and substitute that and $R_{\text{int}}(s, a, s') = \gamma d(s') - d(s)$ into the previous equation, we can get:

$$\begin{aligned} \hat{Q}_{\tilde{M}}(s, a) &= \mathbb{E}_{s'} \left[R(s, a, s') + \lambda R_{\text{int}}(s, a, s') + \gamma \max_{a' \in \mathcal{A}} \hat{Q}_{\tilde{M}}(s', a') \right] \\ &= \mathbb{E}_{s'} \left[R'(s, a, s') + \gamma \max_{a' \in \mathcal{A}} \hat{Q}_{\tilde{M}}(s', a') \right], \end{aligned} \quad (17)$$

which is exactly the Bellman optimality equation for the transformed MDP \tilde{M} , where $\tilde{R} = R + \lambda R_{\text{int}}$ is the reward function for M' . Thus, $Q_{\tilde{M}}^*(s, a) = \hat{Q}_{\tilde{M}}(s, a) = Q_M^*(s, a) - \lambda d(s)$, and the optimal policy for M' therefore satisfies:

$$\begin{aligned} \pi_{\tilde{M}}^*(s) &= \arg \max_{a \in \mathcal{A}} Q_{\tilde{M}}^*(s, a) \\ &= \arg \max_{a \in \mathcal{A}} [Q_M^*(s, a) - \lambda d(s)] \\ &= \arg \max_{a \in \mathcal{A}} Q_M^*(s, a), \end{aligned} \quad (18)$$

and is therefore also optimal in M . To show every optimal policy in M is also optimal in \tilde{M} , simply apply the same proof with the roles of M and \tilde{M} interchanged (and using $-R_{\text{int}}$ as the intrinsic reward). This completes the proof. \square

B. Mathematical Derivations

B.1. Deriving the Optimum of the KL-Constrained Reward Maximization Objective

In this appendix, we will derive Eq. 4. Analogous to Eq. 1, we maximize the KL-constrained objective:

$$J(\theta) = \mathbb{E}_{\mathbf{c}, \mathbf{x}_0 \sim \pi(\mathbf{x}_0 | \mathbf{c})} [r(\mathbf{x}_0, \mathbf{c})] - \beta \cdot \mathbb{D}_{\text{KL}} [\pi(\mathbf{x}_0 | \mathbf{c}) || \pi_{\text{ref}}(\mathbf{x}_0 | \mathbf{c})], \quad (19)$$

under any reward function $r(\mathbf{x}_0, \mathbf{c})$, reference model π_{ref} and a general non-parametric policy class. The objective is reformulated as

$$\begin{aligned}
 & \max_{\pi} \mathbb{E}_{\mathbf{c}, \mathbf{x}_0 \sim \pi(\mathbf{x}_0 | \mathbf{c})} [r(\mathbf{x}_0, \mathbf{c})] - \beta \mathbb{D}_{\text{KL}} [\pi(\mathbf{x}_0 | \mathbf{c}) || \pi_{\text{ref}}(\mathbf{x}_0 | \mathbf{c})] \\
 &= \max_{\pi} \mathbb{E}_{\mathbf{c}} \mathbb{E}_{\mathbf{x}_0 \sim \pi(\mathbf{x}_0 | \mathbf{c})} \left[r(\mathbf{x}_0, \mathbf{c}) - \beta \log \frac{\pi(\mathbf{x}_0 | \mathbf{c})}{\pi_{\text{ref}}(\mathbf{x}_0 | \mathbf{c})} \right] \\
 &= \min_{\pi} \mathbb{E}_{\mathbf{c}} \mathbb{E}_{\mathbf{x}_0 \sim \pi(\mathbf{x}_0 | \mathbf{c})} \left[\log \frac{\pi(\mathbf{x}_0 | \mathbf{c})}{\pi_{\text{ref}}(\mathbf{x}_0 | \mathbf{c})} - \frac{1}{\beta} r(\mathbf{x}_0, \mathbf{c}) \right] \\
 &= \min_{\pi} \mathbb{E}_{\mathbf{c}} \mathbb{E}_{\mathbf{x}_0 \sim \pi(\mathbf{x}_0 | \mathbf{c})} \left[\log \frac{\pi(\mathbf{x}_0 | \mathbf{c})}{\frac{1}{Z(\mathbf{c})} \pi_{\text{ref}}(\mathbf{x}_0 | \mathbf{c}) \exp\left(\frac{1}{\beta} r(\mathbf{x}_0, \mathbf{c})\right)} - \log Z(\mathbf{c}) \right], \tag{20}
 \end{aligned}$$

where the partition function is:

$$Z(\mathbf{c}) = \sum_{\mathbf{x}_0} \pi_{\text{ref}}(\mathbf{x}_0 | \mathbf{c}) \exp\left(\frac{1}{\beta} r(\mathbf{x}_0, \mathbf{c})\right). \tag{21}$$

Note that the partition function is a function of only \mathbf{c} and the reference policy π_{ref} , but does not depend on the policy π . We can now define

$$\pi^*(\mathbf{x}_0 | \mathbf{c}) = \frac{1}{Z(\mathbf{c})} \pi_{\text{ref}}(\mathbf{x}_0 | \mathbf{c}) \exp\left(\frac{1}{\beta} r(\mathbf{x}_0, \mathbf{c})\right), \tag{22}$$

which is a valid probability distribution as $\pi^*(\mathbf{x}_0 | \mathbf{c}) \geq 0, \forall \mathbf{x}_0$ and $\sum_{\mathbf{x}_0} \pi^*(\mathbf{x}_0 | \mathbf{c}) = 1$. Next, we can re-organize the objective in Eq. 20 as

$$\min_{\pi} \mathbb{E}_{\mathbf{c}} \mathbb{E}_{\mathbf{x}_0 \sim \pi(\mathbf{x}_0 | \mathbf{c})} \left[\log \frac{\pi(\mathbf{x}_0 | \mathbf{c})}{\frac{1}{Z(\mathbf{c})} \pi_{\text{ref}}(\mathbf{x}_0 | \mathbf{c}) \exp\left(\frac{1}{\beta} r(\mathbf{x}_0, \mathbf{c})\right)} - \log Z(\mathbf{c}) \right] \tag{23}$$

$$= \min_{\pi} \mathbb{E}_{\mathbf{c}} \left[\mathbb{E}_{\mathbf{x}_0 \sim \pi(\mathbf{x}_0 | \mathbf{c})} \left[\log \frac{\pi(\mathbf{x}_0 | \mathbf{c})}{\pi_{\text{ref}}(\mathbf{x}_0 | \mathbf{c})} \right] - \log Z(\mathbf{c}) \right] \tag{24}$$

$$= \mathbb{E}_{\mathbf{c}} [\mathbb{D}_{\text{KL}} [\pi(\mathbf{x}_0 | \mathbf{c}) || \pi^*(\mathbf{x}_0 | \mathbf{c})] - \log Z(\mathbf{c})] \tag{25}$$

$$= \mathbb{E}_{\mathbf{c}} [\mathbb{D}_{\text{KL}} (\pi(\mathbf{x}_0 | \mathbf{c}) || \pi^*(\mathbf{x}_0 | \mathbf{c}))]. \tag{26}$$

Eq. 24 comes from that $Z(\mathbf{c})$ is not a function of \mathbf{x}_0 , and Eq. 26 comes from that $Z(\mathbf{c})$ does not depend on π . Gibbs' inequality establishes that $\mathbb{D}_{\text{KL}}(\pi || \pi^*) \geq 0$, with equality held if and only if the distributions are identical. Hence, we have the optimal solution:

$$\pi(\mathbf{x}_0 | \mathbf{c}) = \pi^*(\mathbf{x}_0 | \mathbf{c}) = \frac{1}{Z(\mathbf{c})} \pi_{\text{ref}}(\mathbf{x}_0 | \mathbf{c}) \exp\left(\frac{1}{\beta} r(\mathbf{x}_0, \mathbf{c})\right), \tag{27}$$

for all \mathbf{c} . This completes the derivation.

B.2. Deriving the Optimal Policy When KL Coefficient Approaches Zero

In this appendix, we will derive Eq. 5 that shows the behavior of the optimal policy π^* as $\beta \rightarrow 0^+$. Let $\mathbf{x}_0^* = \arg \max_{\mathbf{x}_0} r(\mathbf{x}_0, \mathbf{c})$ be the unique global maximum of the reward function r . We can reformulate the distribution to characterize the density at any point \mathbf{x}_0 relative to the density at the global maximum \mathbf{x}_0^* as

$$\frac{\pi^*(\mathbf{x}_0 | \mathbf{c})}{\pi^*(\mathbf{x}_0^* | \mathbf{c})} = \frac{\pi_{\text{ref}}(\mathbf{x}_0 | \mathbf{c})}{\pi_{\text{ref}}(\mathbf{x}_0^* | \mathbf{c})} \exp\left(\frac{r(\mathbf{x}_0, \mathbf{c}) - r(\mathbf{x}_0^*, \mathbf{c})}{\beta}\right). \tag{28}$$

As $\beta \rightarrow 0^+$, we have

- If $\mathbf{x}_0 = \mathbf{x}_0^*$, the exponent is 0, and the ratio is 1.
- If $r(\mathbf{x}_0, \mathbf{c}) < r(\mathbf{x}_0^*, \mathbf{c})$, then $r(\mathbf{x}_0, \mathbf{c}) - r(\mathbf{x}_0^*, \mathbf{c})$ is a negative constant, leading to the fraction $\frac{r(\mathbf{x}_0, \mathbf{c}) - r(\mathbf{x}_0^*, \mathbf{c})}{\beta} \rightarrow -\infty$ and the ratio $\frac{\pi^*(\mathbf{x}_0 | \mathbf{c})}{\pi^*(\mathbf{x}_0^* | \mathbf{c})} \rightarrow 0$.

This implies that for any \mathbf{x}_0 where the reward is not maximal, the relative probability mass drops to zero as

$$\lim_{\beta \rightarrow 0^+} \frac{\pi^*(\mathbf{x}_0 | \mathbf{c})}{\pi^*(\mathbf{x}_0^* | \mathbf{c})} = 0 \quad \text{for all } \mathbf{x}_0 \neq \mathbf{x}_0^*. \quad (29)$$

Because the total probability must integrate to 1, but the density at all non-maximal points vanishes, the entire probability mass must pile up at the location of the maximum reward. Formally, for any smooth test function $f(\mathbf{x}_0)$:

$$\lim_{\beta \rightarrow 0^+} \int \pi^*(\mathbf{x}_0) f(\mathbf{x}_0) d\mathbf{x}_0 = f(\mathbf{x}_0^*). \quad (30)$$

This is the defining property of the Dirac delta distribution $\delta(\mathbf{x}_0 - \mathbf{x}_0^*)$. This completes the proof.

C. Quantifying Intra-Group Diversity

The most straightforward choice for the pre-trained encoder \mathcal{E} in Eq. 10 is a variational auto-encoder (VAE), which serves as the de facto standard for obtaining latent representations in modern diffusion models (Rombach et al., 2022). However, such encoders may fail to capture meaningful perceptual or semantic variations in generated images. Instead, we utilize DreamSim (Fu et al., 2023), a model trained by concatenating CLIP, OpenCLIP, and DINO embeddings, and subsequently fine-tuned on human perceptual judgments. DreamSim is particularly well-suited for RFT that typically addresses downstream objectives like text-image alignment and human-centric evaluation. To this end, we design a simple, easy-to-implement metric to quantify image diversity using image-level representations extracted from an off-the-shelf pre-trained encoder. As a general framework, our method is also compatible with any other diversity metrics.

D. Computation of diversity evaluation metrics

We construct the generation image set using a fixed set of prompts and a controlled sampling protocol. Specifically, we select 40 representative prompts from the evaluation set, ensuring consistency across all methods evaluated, including both the base model and the fine-tuned models. For each prompt, we generate 40 images using identical random seeds across different models, resulting in a total of 1,600 generated images per method.

Dreamsim diversity uses the dreamsim library (Fu et al., 2023) to compute Dreamsim diversity as the variance of Dreamsim embeddings of 40 generations for a given prompt, averaged across 40 prompts. Namely,

$$\text{Dreamsim_diversity} = \frac{1}{40} \sum_{k=1}^{40} \frac{2}{40 \cdot 39} \sum_{1 \leq i < j \leq 40} \left\| \text{Dreamsim}(\mathbf{o}_i^k) - \text{Dreamsim}(\mathbf{o}_j^k) \right\|^2, \quad (31)$$

where \mathbf{o}_i^k denotes the i -th generation for the k -th prompt. A higher DreamSim Diversity value indicates greater variation among generated samples, reflecting higher generative diversity.

ClipScore diversity uses the open_clip library (Ilharco et al., 2021) to compute ClipScores. ClipScore diversity is computed in analogy with Dreamsim diversity.

Generalized Recall (Sajjadi et al., 2018) introduces the classic concepts of precision and recall to the study of generative models, providing distinct conclusions that are otherwise confounded by metrics like FID. While high precision implies a higher degree of realism and fidelity of the images compared to the base distribution, high recall implies higher coverage of the data distribution by the generator, signifying diversity. The approach proposed (e.g., (Kynkänniemi et al., 2019)) forms non-parametric representations of the data manifolds using overlapping hyperspheres defined by the k-Nearest Neighbors (kNN) technique. Following this method, binary assignments are used to compute the recall. We specifically compute the recall of the generated distribution with respect to the distribution of the base model, which covers multiple modes of the dataset. For our experiments, the neighborhood size is set to $k = 10$.

Vendi Score ((Friedman & Dieng, 2022)) is a diversity metric that quantifies the effective number of distinct modes captured by a set of images. Unlike distance-based metrics, the Vendi Score provides a single value that represents the effective rank or intrinsic dimensionality of the generated feature distribution. It operates by first extracting high-dimensional feature embeddings from the images. These embeddings are then used to construct a kernel matrix K , where each entry K_{ij}

measures the similarity between samples i and j . The score is computed by applying a mathematical function (specifically, the effective rank calculation) to the eigenvalues λ_i of this normalized kernel matrix, often using the exponential of the negative entropy of the eigenvalues:

$$\text{Vendi}(\mathbf{E}) = \exp \left(- \sum_i p_i \ln p_i \right), \quad \text{where } p_i = \frac{\lambda_i}{\sum_j \lambda_j}$$

A higher Vendi Score indicates greater diversity, as it implies that the images are more spread out in the feature space, corresponding to a higher effective number of captured modes. The metric is invariant to the sample size, making it a robust measure for comparing the diversity of different generative models. We compute the pairwise distances based on the absolute value of the reward function. Specifically, the pairwise distances are given by:

E. Details of Reward-Based Sample Selection

This appendix provides implementation details of the reward-based sample selection strategies used to construct training batches in our GRPO fine-tuning experiments. For each prompt, the policy generates a pool of $2G$ candidate outputs $\{\mathbf{o}_1, \dots, \mathbf{o}_{2G}\}$, from which G samples are selected to form the effective training batch. We compute the pairwise distances based on the absolute value of the reward function. Specifically, the pairwise distances D_{ij} are given by:

$$D_{ij} = |R(\mathbf{o}_i, \mathbf{o}_j)|$$

where $R(\mathbf{o}_i, \mathbf{o}_j)$ is the reward function that measures the relationship between samples \mathbf{o}_i and \mathbf{o}_j , $|R(\mathbf{o}_i, \mathbf{o}_j)|$ represents the absolute value of the reward, which quantifies the strength of the relationship between \mathbf{o}_i and \mathbf{o}_j in a task-specific way. This results in a reward-based distance matrix $\mathbf{D} \in \mathbb{R}^{2G \times 2G}$, where the entries are based on the pairwise absolute values of the rewards.

Reward-Concentrated Selection. This strategy selects G samples that are close to each other in the reward distance by using a nearest-neighbor criterion. For each candidate i , we retrieve the indices of its $G - 1$ nearest neighbors and compute the corresponding distance sum

$$s_i = \sum_{j \in \min(i; G-1)} D_{ij}, \quad (32)$$

where $\min(i; G - 1)$ denotes the set of indices of the $G - 1$ nearest distances in row i . We choose the reference index $i^* = \arg \min_i s_i$ and form the training batch by including this reference sample together with its $G - 1$ nearest neighbors.

Reward-Contrasted Selection. This strategy selects G samples that are well separated in the reward distance by using a farthest-neighbor criterion. For each candidate i , we retrieve its $G - 1$ farthest neighbors and compute the corresponding distance sum

$$t_i = \sum_{j \in \max(i; G-1)} D_{ij}, \quad (33)$$

where $\max(i; G - 1)$ denotes the set of indices of the $G - 1$ largest distances in row i . We choose the reference index $i^* = \arg \max_i t_i$ and form the training batch by including this reference sample together with its $G - 1$ farthest neighbors.

All other training components are kept identical across settings, with the two strategies differing only in how G samples are selected from the $2G$ candidate pool.

F. Annealed Prompt Embedding Noise

Our noise-conditioned prompting strategy is inspired by the Condition-Annealed Diffusion Sampler (CADS) (Sadat et al., 2024), which introduces timestep-dependent perturbations to conditioning signals during diffusion inference to promote generative diversity. CADS applies stronger perturbations at early diffusion steps and gradually reduces them as inference progresses, aligning stochasticity with the diffusion dynamics.

Following this principle, we inject timestep-annealed noise into the prompt embeddings during generation of training. Let y denote the clean prompt embedding. At the diffusion timestep t , we construct a perturbed prompt embedding \tilde{e}_t as

$$\tilde{e}_t = \sqrt{\gamma(t)} e + s\sqrt{1 - \gamma(t)} n, \quad n \sim \mathcal{N}(0, I), \quad (34)$$

where s controls the overall noise scale and $\gamma(t) \in [0, 1]$ is an annealing function that decreases with the diffusion timestep. We adopt a piecewise linear annealing schedule for $\gamma(t)$:

$$\gamma(t) = \begin{cases} 1, & t \leq \tau_1, \\ \frac{\tau_2 - t}{\tau_2 - \tau_1}, & \tau_1 < t < \tau_2, \\ 0, & t \geq \tau_2, \end{cases} \quad (35)$$

where τ_1 and τ_2 are user-defined thresholds that determine the transition from high to low noise. Since diffusion inference proceeds backward in time, this schedule applies stronger perturbations at earlier timesteps and gradually removes noise as generation converges.

Adding noise to the prompt embeddings alters their mean and variance, which can lead to instability when the noise scale is large. To mitigate this effect, we apply a rescaling operation similar to that used in CADS. Specifically, given a noisy embedding \tilde{e}_t with empirical mean and standard deviation $\mu(\tilde{e}_t)$ and $\sigma(\tilde{e}_t)$, we compute a rescaled embedding

$$\tilde{e}_t^{\text{rescaled}} = \frac{\tilde{e}_t - \mu(\tilde{e}_t)}{\sigma(\tilde{e}_t)} \sigma_e + \mu_e, \quad (36)$$

where μ_e and σ_e denote the mean and standard deviation of the clean prompt embeddings. The final prompt embedding is then obtained by mixing the rescaled and unrescaled embeddings:

$$\tilde{e}_t^{\text{final}} = \psi \tilde{e}_t^{\text{rescaled}} + (1 - \psi) \tilde{e}_t, \quad (37)$$

where $\psi \in [0, 1]$ controls the strength of rescaling. This rescaling strategy improves numerical stability under high noise levels while preserving sufficient stochasticity for diversity enhancement. Unlike CADS, which applies condition annealing purely at inference time, our formulation integrates timestep-annealed prompt embedding noise into reinforcement learning fine-tuning, explicitly diversifying the conditioning space explored during optimization and helping mitigate diversity collapse. In our experiments, the noise scale is set to $s = 0.05$, the annealing thresholds are $\tau_1 = 0.4$ and $\tau_2 = 1.0$ (with timesteps normalized to $[0, 1]$), and the rescaling mixing factor is $\psi = 1$, which we found to work well in practice.

G. Implementation Details

We perform training on 45 common animals using two reward functions, PickScore and HPSv2, as shown in Table 3. The hyperparameter settings for each reward are listed in Table 2. All experiments are conducted on a system with two NVIDIA RTX 4090 GPUs, using FP16 mixed-precision training with automatic mixed precision (AMP) and gradient scaling for improved computational efficiency and reduced memory consumption. The KL ratio β is set to 0.001 for GRPO-KL. We use LoRA with $\alpha = 16$ and $r = 8$ for all methods.

H. Reward Models

We use two human-preference-based reward models, HPSv2 and PickScore, to provide external reward feedback during training. Both models are trained to predict pairwise preferences between images generated from the same prompt.

HPSv2 is trained on a dataset containing approximately 434k images organized into pairwise comparisons. Each comparison consists of two images generated by different models using the same prompt and is annotated with a binary preference choice provided by a single annotator. The prompts are collected from DrawBench and DiffusionDB, where prompts from DiffusionDB are further sanitized using ChatGPT to reduce biases introduced by stylistic trigger words and to lower the overall NSFW score. This preprocessing results in a more controlled prompt distribution for training the reward model.

PickScore is trained on the Pick-a-Pic dataset, which is collected through a web-based application. Users are allowed to freely write prompts and are presented with two generated images per prompt. They are asked to select their preferred image or indicate a tie if no strong preference exists. While moderation is applied to remove users who generate NSFW content or

Table 2. List of hyperparameter configurations for PickScore and HPSv2.

| Hyperparameters | PickScore | HPSv2 |
|------------------------------------|--------------------|--------------------|
| Random seed | 42 | 42 |
| Denoising timesteps (T) | 50 | 50 |
| group size (G) | 8 | 8 |
| Guidance scale | 5.0 | 5.0 |
| Policy learning rate | 1×10^{-4} | 1×10^{-4} |
| Policy clipping range | 1×10^{-4} | 1×10^{-4} |
| Maximum gradient norm | 1.0 | 1.0 |
| Optimizer | AdamW | AdamW |
| Optimizer weight decay | 1×10^{-4} | 1×10^{-4} |
| Optimizer β_1 | 0.9 | 0.9 |
| Optimizer β_2 | 0.999 | 0.999 |
| Optimizer ϵ | 1×10^{-8} | 1×10^{-8} |
| Sampling batch size | 16 | 16 |
| Samples per epoch | 256 | 256 |
| Training batch size | 2 | 2 |
| Gradient accumulation steps | 16 | 16 |
| Training steps per epoch | 64 | 64 |
| Gradient updates per epoch | 4 | 4 |
| noise level α | 1.0 | 1.0 |
| shaping ratio λ | 0.5 | 0.5 |
| predetermined upper bound σ | 1.0 | 1.0 |

Table 3. List of 45 animals as training prompts on PickScore and HPSv2.

| | | | | | | | | |
|--------|--------|-------|-----------|--------|---------|---------|----------|----------|
| cat | dog | horse | monkey | rabbit | zebra | spider | bird | sheep |
| deer | cow | goat | lion | tiger | bear | raccoon | fox | wolf |
| lizard | beetle | ant | butterfly | fish | shark | whale | dolphin | squirrel |
| mouse | rat | snake | turtle | frog | chicken | duck | goose | bee |
| pig | turkey | fly | llama | camel | bat | gorilla | hedgehog | kangaroo |

exhibit low-quality annotation behavior (e.g., extremely rapid or random choices), the dataset still contains a notable amount of NSFW prompts. As a result, fine-tuning with PickScore may lead to an increased tendency to generate NSFW images, even when the input prompts are not explicitly NSFW.